Acta Cryst E CRYSTALLOGRAPHIC COMMUNICATIONS

ISSN 2056-9890

Crystal structure, Hirshfeld surface analysis and interaction energy and DFT studies of 1-(1,3-benzothiazol-2-yl)-3-(2-hydroxyethyl)imidazolidin-2-one

Mohamed Srhir,[a]* Nada Kheira Sebbar,[b,a] Tuncer Hökelek,[c] Ahmed Moussaif,[a] Joel T. Mague,[d] Noureddine Hamou Ahabchane[a] and El Mokhtar Essassi[a]

[a]Laboratoire de Chimie Organique Hétérocyclique URAC 21, Pôle de Compétence Pharmacochimie, Av. Ibn Battouta, BP 1014, Faculté des Sciences, Université Mohammed V, Rabat, Morocco, [b]Faculté des Sciences Appliquées Ait Melloul, Université Ibn Zohr, Agadir, Morocco, [c]Department of Physics, Hacettepe University, 06800 Beytepe, Ankara, Turkey, and [d]Department of Chemistry, Tulane University, New Orleans, LA 70118, USA. *Correspondence e-mail: mohamedsrhir2018@gmail.com

Received 23 December 2019
Accepted 6 February 2020

Edited by J. Jasinsk, Keene State College, USA

Keywords: crystal structure; benzothiazine; hydrogen bond; triazole; π-stacking; Hirshfeld surface.

CCDC reference: 1982595

Supporting information: this article has supporting information at journals.iucr.org/e

In the title molecule, $C_{12}H_{13}N_3O_2S$, the benzothiazine moiety is slightly non-planar, with the imidazolidine portion twisted only a few degrees out of the mean plane of the former. In the crystal, a layer structure parallel to the *bc* plane is formed by a combination of $O-H_{Hydethy}\cdots N_{Thz}$ hydrogen bonds and weak $C-H_{Imdz}\cdots O_{Imdz}$ and $C-H_{Bnz}\cdots O_{Imdz}$ (Hydethy = hydroxyethyl, Thz = thiazole, Imdz = imidazolidine and Bnz = benzene) interactions, together with $C-H_{Imdz}\cdots\pi$(ring) and head-to-tail slipped π-stacking [centroid-to-centroid distances = 3.6507 (7) and 3.6866 (7) Å] interactions between thiazole rings. The Hirshfeld surface analysis of the crystal structure indicates that the most important contributions for the crystal packing are from H···H (47.0%), H···O/O···H (16.9%), H···C/C···H (8.0%) and H···S/S···H (7.6%) interactions. Hydrogen bonding and van der Waals interactions are the dominant interactions in the crystal packing. Computational chemistry indicates that in the crystal, C—H···N and C—H···O hydrogen-bond energies are 68.5 (for $O-H_{Hydethy}\cdots N_{Thz}$), 60.1 (for $C-H_{Bnz}\cdots O_{Imdz}$) and 41.8 kJ mol^{-1} (for $C-H_{Imdz}\cdots O_{Imdz}$). Density functional theory (DFT) optimized structures at the B3LYP/6–311 G(d,p) level are compared with the experimentally determined molecular structure in the solid state.

1. Chemical context

Compounds containing the benzothiazole backbone have been studied extensively in both academic and industrial laboratories (Mekhzoum *et al.*, 2016, 2019; Chakib *et al.*, 2010*a*,*b*, 2019). These molecules exhibit a wide range of biological applications including as anti-tumor agents (Béneteau *et al.*, 1999; Ćaleta *et al.*, 2004), antimicrobial agents (Shastry *et al.*, 2003; Latrofa *et al.*, 2005, Singh *et al.*, 2013), analgesics (Kaur *et al.*, 2010), anti-inflammatory agents (Oketani *et al.*, 2001), anti-HIV agents (Nagarajan *et al.*, 2003; Pitta *et al.*, 2013), anti-leishmanial agents (Delmas *et al.*, 2004), anti-cancer agents (Yang *et al.*, 2003; Huang *et al.*, 2006; Kok *et al.*, 2008), anti-hypertensive agents (Saggu *et al.*, 2002), anti-oxidants, (Ayhan-Kilcigil *et al.*, 2004) and anti-viral agents (Tewari *et al.*, 2006). The imidazolinone moiety is an important scaffold possessing a spectrum of pharmacological actions, which include anti-convulsant, anti-parkinsonism and mono-amino-oxidase inhibitory activities (Hari Narayana Moorthy

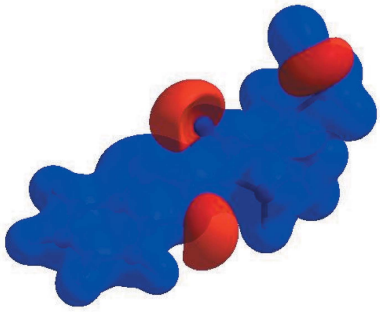

OPEN ACCESS

et al., 2012; Desai *et al.*, 2009). Furthermore, imidazolones are anti-bacterial, anti-fungal, anti-viral, anti-cancer and CNS-depressant agents (Naithani *et al.*, 1989; Harfenist *et al.*, 1978). We have previously shown that bis(2-chloroethyl)amine hydrochloride is an interesting precursor of several heterocyclic compounds containing the oxazolidinone moiety (Sebbar *et al.*, 2016, 2018; Ellouz *et al.*, 2017; Hni *et al.*, 2019). In a continuation of our research using bis(2-chloroethyl)amine hydrochloride as an intermediate in the synthesis of new heterocyclic systems, we have studied the condensation of 2-aminobenzothiazole with bis(2-chloroethyl)amine hydrochloride in the presence of tetra-*n*-butylammonium bromide as catalyst and potassium carbonate as base. A plausible mechanism for the formation of the product, 1-(1,3-benzothiazol-2-yl)-3-(2-hydroxyethyl)-imidazolidin-2-one (**I**), is given in the reaction scheme.

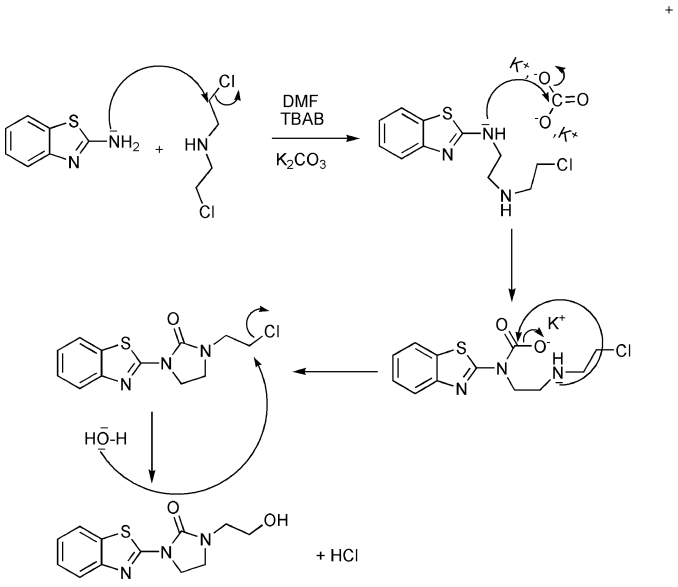

The title compound was obtained for the first time and characterized by single crystal X-ray diffraction techniques as well as by Hirshfeld surface analysis. The results of the calculations by density functional theory (DFT), carried out at the B3LYP/6-311G (d,p) level, are compared with the experimentally determined molecular structure in the solid state.

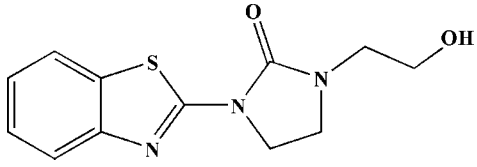

2. Structural commentary

In the title molecule (**I**) (Fig. 1), the benzothiazole unit is slightly non-planar, as indicated by the dihedral angle of 1.52 (4)° between the mean planes of the component rings, [*A* (C1–C6) and *B* (S1/N1/C1/C6/C7)]. A puckering analysis of the conformation of the imidazolidine ring *C* (N2/N3/C8-C10) gave the parameters $Q(2)$ = 0.0767 (14) Å and $\varphi(2)$ = 66.5 (10)°. The conformation is described as an 'envelope on C9′. This ring is almost coplanar with the thiazole ring *B* with a dihedral angle of 3.61 (4)° between their mean planes.

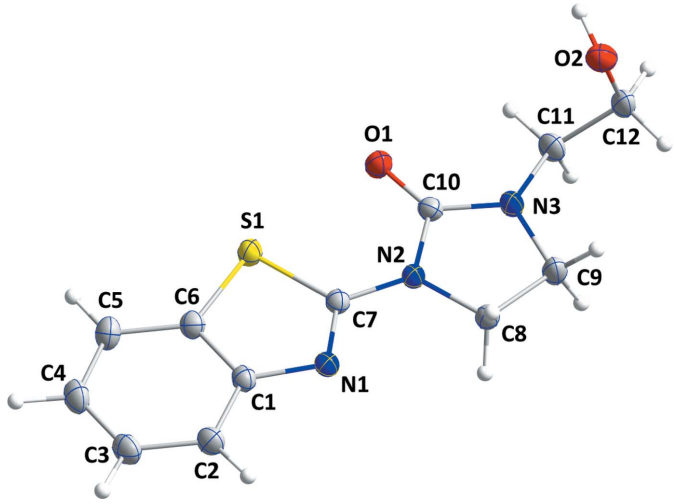

Figure 1
The molecular structure of the title compound with the atom-numbering scheme. Displacement ellipsoids are drawn at the 50% probability level.

3. Supramolecular features

In the crystal, $O-H_{Hydethy}\cdots N_{Thz}$ (Hydethy = hydroxyethyl and Thz = thiazole) hydrogen bonds (Table 1) form stepped chains of molecules extending along the *c*-axis direction (Fig. 2). These are connected into layers parallel to the *bc* plane by weak $C-H_{Imdz}\cdots O_{Imdz}$ (Imdz = imidazolidine) and $C-H_{Imdz}\cdots\pi$(ring) interactions (Table 1). The layers are connected by weak $C-H_{Bnz}\cdots O_{Imdz}$ (Bnz = benzene) interactions. Both the layer formation and stacking are also assisted by head-to-tail slipped π-stacking interactions (Figs. 3 and 4)

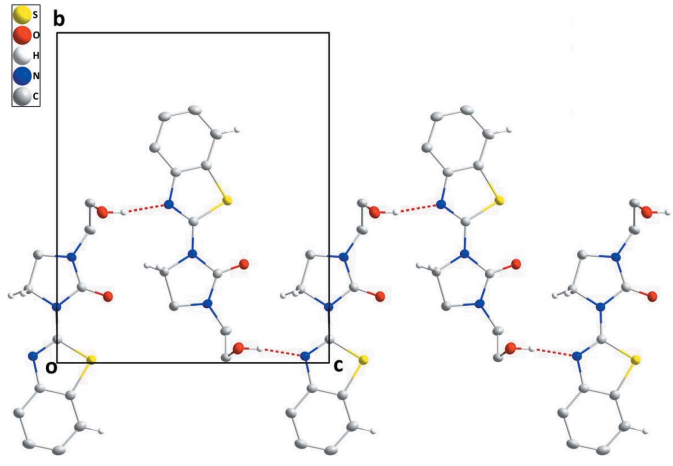

Figure 2
A portion of the $O-H_{Hydethy}\cdots N_{Thz}$ (Hydethy = hydroxyethyl and Thz = thiazole) (red dashed lines) hydrogen bonded chain in **I** viewed along the *a* axis.

Table 1
Hydrogen-bond geometry (Å, °).

*Cg*1 is the centroid of the benzene ring (*A*, C1–C6).

D—H···*A*	*D*—H	H···*A*	*D*···*A*	*D*—H···*A*
O2—H2*A*···N1^{iii}	0.90 (2)	1.97 (2)	2.8560 (15)	170 (2)
C5—H5···O1^{i}	0.954 (19)	2.559 (19)	3.4439 (16)	154.3 (14)
C8—H8*B*···O1^{vi}	0.958 (17)	2.532 (16)	3.2542 (16)	132.2 (13)
C8—H8*A*···*Cg*1^{iv}	0.997 (17)	2.840 (16)	3.5646 (15)	130.0 (12)

Symmetry codes: (i) $-x+2, y+\frac{1}{2}, -z+\frac{3}{2}$; (iii) $x, -y+\frac{1}{2}, z+\frac{1}{2}$; (iv) $-x+1, -y+1, -z+1$; (vi) $x, -y+\frac{1}{2}, z-\frac{1}{2}$.

along the *a*-axis direction between thiazole rings [*Cg*2···*Cg*2^{i} and *Cg*2···*Cg*2^{ii} = 3.6507 (7) and 3.6866 (7) Å, respectively; symmetry codes: (i) $-x+1, -y+1, -z+1$; (ii) $-x+2, -y+\frac{1}{2}, -z+\frac{3}{2}$, where *Cg*2 is the centroid of ring *B*].

4. Hirshfeld surface analysis

In order to visualize the intermolecular interactions in the crystal of **I**, a Hirshfeld surface (HS) analysis (Hirshfeld, 1977; Spackman & Jayatilaka, 2009) was carried out using *Crystal Explorer 17.5* (Turner *et al.*, 2017). In the HS plotted over d_{norm} (Fig. 5), the white surface indicates contacts with distances equal to the sum of van der Waals radii, and the red and blue colours indicate distances shorter (in close contact) or longer (distant contact) than the van der Waals radii, respectively (Venkatesan *et al.*, 2016). The bright-red spots appearing near O1 and hydrogen atoms H5, H2*A*, H8*B* indicate their roles as donors and/or acceptors; they also appear as blue and red regions corresponding to positive and negative potentials on the HS mapped over electrostatic potential (Spackman *et al.*, 2008; Jayatilaka *et al.*, 2005) shown in Fig. 6. The blue regions indicate positive electrostatic potential (hydrogen-bond donors), while the red regions indicate negative electrostatic potential (hydrogen-bond acceptors).

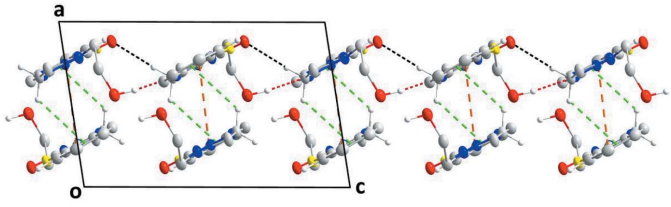

Figure 3
Portions of two chains, viewed along the *b* axis, showing the interactions between them. O—$H_{Hydethy}$···N_{Thz} hydrogen bonds are shown by red dashed lines while the weak C—H_{Imdz}···O_{Imdz} and C—H_{Bnz}···O_{Imdz} (Hydethy = hydroxyethyl, Thz = thiazole, Imdz = imidazolidine and Bnz = benzene) interactions are shown by black dashed lines. The weak C—H_{Imdz}···π(ring) and the head-to-tail slipped π-stacking interactions are shown, respectively, by green and orange dashed lines.

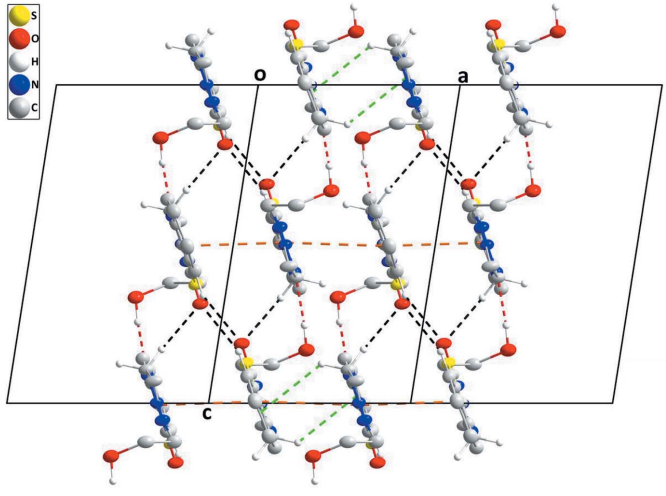

Figure 4
A partial packing diagram viewed along the *b* axis with intermolecular interactions depicted as in Fig. 3. Three unit cells along the *a* axis are shown.

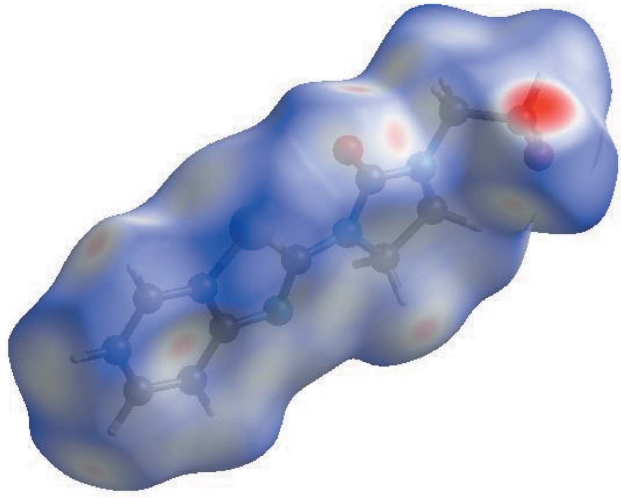

Figure 5
View of the three-dimensional Hirshfeld surface of **I** plotted over d_{norm} in the range −0.5793 to 1.2827 a.u.

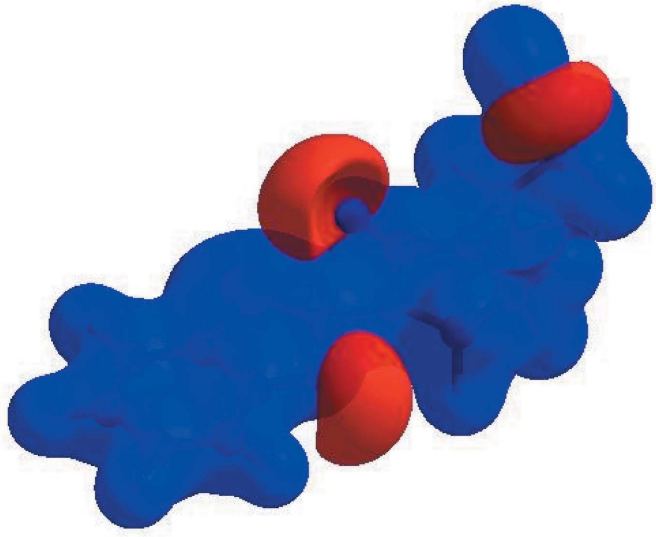

Figure 6
View of the three-dimensional Hirshfeld surface of **I** plotted over electrostatic potential energy in the range −0.0500 to 0.0500 a.u. using the STO-3 G basis set at the Hartree–Fock level of theory. Hydrogen-bond donors and acceptors are shown as blue and red regions around the atoms corresponding to positive and negative potentials, respectively.

Table 2
Selected interatomic distances (Å).

S1···O1	2.7721 (10)	C1···C7^{iv}	3.4070 (17)
S1···C11^{i}	3.6700 (14)	C2···C10^{iv}	3.5859 (18)
S1···C1^{ii}	3.6552 (12)	C3···C10^{iv}	3.5928 (19)
S1···H11*A*^{i}	3.117 (16)	C4···C10^{ii}	3.4350 (19)
O1···C9^{iii}	3.2869 (16)	C4···C8^{iv}	3.587 (2)
O1···C8^{iii}	3.2543 (16)	C6···C7^{ii}	3.5502 (17)
O2···N1^{iii}	2.8560 (14)	C1···H2*A*^{vi}	2.81 (2)
O2···C3^{iv}	3.4071 (17)	C4···H8*A*^{iv}	2.850 (16)
O2···N3	2.9500 (15)	C5···H8*A*^{iv}	2.718 (15)
O1···H9*B*^{iii}	2.640 (17)	C9···H12*B*	2.830 (16)
O1···H11*A*	2.482 (17)	C12···H9*A*	2.857 (18)
O1···H8*B*^{iii}	2.534 (16)	H2···H9*A*^{vii}	2.49 (3)
O2···H9*A*^{v}	2.804 (19)	H2···H2*A*^{vi}	2.53 (3)
O2···H12*B*^{v}	2.803 (18)	H2*A*···H8*B*^{iii}	2.59 (3)
O2···H3^{iv}	2.601 (18)	H4···C12^{viii}	2.828 (18)
O2···H2^{iii}	2.838 (18)	H4···H12*A*^{viii}	2.38 (2)
N1···C12^{vi}	3.4313 (17)	H4···H12*B*^{viii}	2.38 (2)
N2···C5^{ii}	3.4204 (17)	H5···O1^{i}	2.557 (17)
N1···H8*B*	2.769 (17)	H5···H11*A*^{i}	2.36 (2)
N1···H2*A*^{vi}	1.97 (2)	H8*B*···H11*A*^{vi}	2.44 (2)
N1···H8*A*	2.857 (17)	H9*A*···H12*B*	2.40 (2)

Symmetry codes: (i) $-x+2, y+\frac{1}{2}, -z+\frac{3}{2}$; (ii) $-x+2, -y+1, -z+1$; (iii) $x, -y+\frac{1}{2}, z+\frac{1}{2}$; (iv) $-x+1, -y+1, -z+1$; (v) $-x+1, -y, -z+1$; (vi) $x, -y+\frac{1}{2}, z-\frac{1}{2}$; (vii) $-x+1, y+\frac{1}{2}, -z+\frac{1}{2}$; (viii) $x, y+1, z$.

The shape-index of the HS is a tool to visualize π–π stacking by the presence of adjacent red and blue triangles; if there are no adjacent red and/or blue triangles, then there are no π–π interactions. Fig. 7 clearly suggests that there are π–π interactions in **I**.

The overall two-dimensional fingerprint plot, Fig. 8*a*, and those delineated into H···H, H···O/O···H, H···C/C···H, H···S/S···H, H···N/N ··· H, C···C, N···C/C···N, O···C/C···O, S···C/C···S and S···N/N ··· S contacts (McKinnon *et al.*, 2007) are illustrated in Fig. 8*b*–*k*, respectively, together with their relative contributions to the Hirshfeld surface. The most important interaction (Table 2) is H···H, contributing 47.0% to the overall crystal packing, which is reflected in Fig. 8*b* as widely scattered points of high density due to the large hydrogen content of the molecule with the tip at $d_e = d_i$ = 1.10 Å. The pair of wings in the fingerprint plot delineated into H···O/O···H contacts (Fig. 8*c*, 16.9% contribution) has a symmetrical distribution of points with the edges at $d_e + d_i$ = 2.40 Å. The presence of C—H···π interactions is indicated by the characteristic wings with a spikes with the tips at $d_e + d_i$ = 2.63 Å in the fingerprint plot delineated into H···C/C···H contacts (Fig. 8*d*, 8.0% contribution). The H···S/S···H contacts contribute 7.6% to the overall crystal packing and are seen in Fig. 8*e* as widely scattered points with the tips at $d_e + d_i$ = 3.03 Å. The pair of spikes in the fingerprint plot delineated into H···N/N···H contacts (Fig. 8*f*, 5.3%) has a symmetrical distribution of points with the tips at $d_e + d_i$ = 1.88 Å. The C···C contacts (5.0% contribution, Fig. 8*g*) have an arrow-shaped distribution of points with the tip at $d_e = d_i$ = 1.70 Å. The N···C/C···N interactions (4.3%, Fig. 8*h*) give rise to tiny wings with the tips at $d_e + d_i$ = 3.41 Å. The O···C/C···O contacts (2.2%, Fig. 8*i*) give widely scattered points with the tips at $d_e + d_i$ = 3.56 Å. Finally, the S···C/C···S and S···N/N···S interactions, contributing 2.2% and 1.3% to the overall crystal packing (Fig. 8*j* and *k*) give rise to tiny wings with the tips at $d_e + d_i$ = 3.63 Å and $d_e + d_i$ = 3.63 Å, respectively.

The Hirshfeld surface representations with the function d_{norm} plotted onto the surface are shown for the H···H,

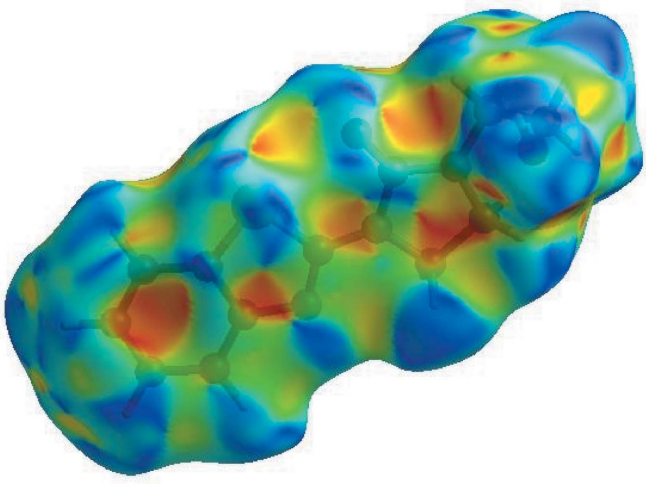

Figure 7
Hirshfeld surface of **I** plotted over shape-index.

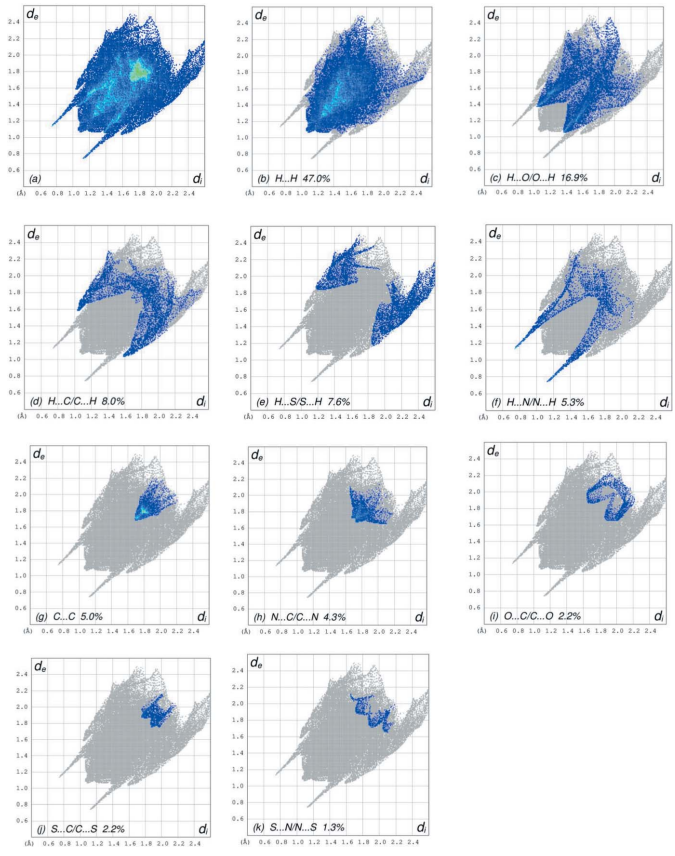

Figure 8
The full two-dimensional fingerprint plots for **I**, showing (*a*) all interactions, and those delineated into (*b*) H···H, (*c*) H···O/O···H, (*d*) H···C/C···H, (*e*) H···S/S···H, (*f*) H···N/N···H, (*g*) C···C, (*h*) C···N/N···C, (i) O···C/C···O, (*j*) S···C/C···S and (*k*) S···N/N···S interactions. The d_i and d_e values are the closest internal and external distances (in Å) from given points on the Hirshfeld surface.

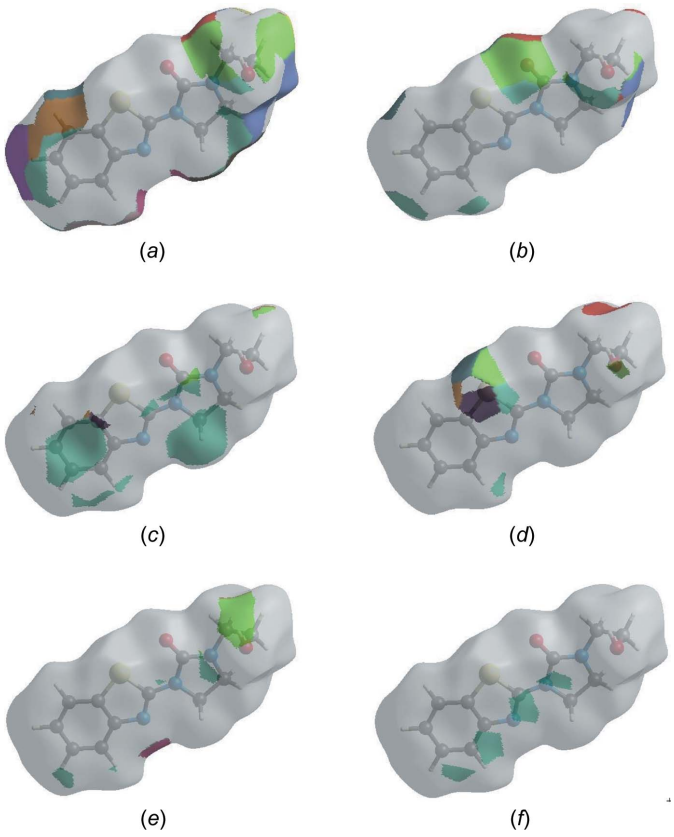

Figure 9
The Hirshfeld surface representations for **I** with the function d_{norm} plotted onto the surface for (*a*) H···H, (*b*) H···O/O···H, (*c*) H···C/C···H, (*d*) H···S/S···H, (*e*) H···N/N···H and (*f*) C···C interactions.

H···O/O···H, H···C/C···H, H···S/S···H, H···N/N···H and C···C interactions in Fig. 9*a*--*f*, respectively.

The Hirshfeld surface analysis confirms the importance of H-atom contacts in establishing the packing. The large number of H···H, H···O/O···H and H···C/C···H interactions suggest that van der Waals interactions and hydrogen bonding play the major roles in the crystal packing (Hathwar *et al.*, 2015).

5. Interaction energy calculations

The intermolecular interaction energies were calculated by the CE–B3LYP/6–311G(d,p) energy model available in *Crystal Explorer 17.5* (Turner *et al.*, 2017) using the cluster of molecules generated by applying crystallographic symmetry operations within a radius of 3.8 Å of a central molecule (Turner *et al.*, 2014). The total intermolecular energy (E_{tot}) is the sum of electrostatic (E_{ele}), polarization (E_{pol}), dispersion (E_{dis}) and exchange-repulsion (E_{rep}) energies (Turner *et al.*, 2015) with scale factors of 1.057, 0.740, 0.871 and 0.618, respectively (Mackenzie *et al.*, 2017). Hydrogen-bonding interaction energies (in kJ mol^{-1}) were calculated to be −67.2 (E_{ele}), −18.0 (E_{pol}), −35.4 (E_{dis}), 75.7 (E_{rep}) and −68.5 (E_{tot}) for O2—H2*A*···N1, −21.5 (E_{ele}), −6.1 (E_{pol}), −82.0 (E_{dis}), 62.3 (E_{rep}) and −60.1 (E_{tot}) for C5—H5···O1 and −1.2 (E_{ele}), −6.3 (E_{pol}), −73.7 (E_{dis}), 45.7 (E_{rep}) and −41.8 (E_{tot}) for C8—H8*B*···O1.

Table 3
Comparison of the selected (X-ray and DFT) geometric data (Å, °).

Bonds/angles	X-ray	B3LYP/6–311G(d,p)
S1—C6	1.7448 (13)	1.83061
S1—C7	1.7517 (12)	1.85613
O1—C10	1.2246 (16)	1.24399
O2—C12	1.4161 (17)	1.45513
N1—C7	1.3060 (16)	1.30197
N1—C1	1.3940 (16)	1.40321
N2—C7	1.3619 (17)	1.37118
N2—C10	1.3930 (16)	1.40686
N2—C8	1.4628 (16)	1.47735
N3—C10	1.3477 (16)	1.37333
N3—C11	1.4485 (16)	1.45760
N3—C9	1.4543 (17)	1.47023
C6—S1—C7	88.16 (6)	87.72
C7—N2—C10	125.18 (10)	126.57
C7—N1—C1	109.77 (10)	110.27
C7—N2—C8	122.65 (10)	121.09
C10—N2—C8	112.16 (10)	112.17
C10—N3—C11	123.10 (11)	122.39
C10—N3—C9	113.37 (10)	113.06
C11—N3—C9	122.24 (11)	123.84

6. DFT calculations

The main aim of these computations is to provide an interpretation of the experimental results. For this purpose, the structural parameters of equilibrium geometry for **I** in the gas phase have been computed using the B3LYP functional level of theory and the 6-31G (d,p) basis set (Becke, 1993) implemented in *GAUSSIAN-09* (Frisch *et al.*, 2009). The molecule adopts a geometry very close to that obtained using DFT calculations (Table 3). The largest differences between the calculated and experimental values are observed for the S1—C6 (0.1 Å) and S1—C7 (0.08 Å) bond lengths and the C11—N3—C9 bond angle (1.6°). These disparities can be linked to the fact that these calculations relate to the isolated molecule, whereas the experimental results correspond to interacting molecules in the crystal lattice where intra and intermolecular interactions with the neighboring molecules are present.

7. Database survey

A search of the Cambridge Structural Database (CSD, Version 5.41 updated to December 2019; Groom *et al.*, 2016) with the search fragment **II** generated 24 hits of which 10 were metal complexes of benzothiazole or its derivatives. Of the remaining molecules, the four closest in composition and structure to **I** are **III** (KEQTAC; Olyaei *et al.*, 2006), **IV** (NOHJAX; Sahoo *et al.*, 2014), **V** (RUBPAG; Saczewski *et al.*, 2005) and **VI** (YUYTUH; Kozísek *et al.*, 1995). In all four, the benzothiazole moiety is more nearly planar than in **I**, with the dihedral angle between the constituent planes being < 1° except for **VI** where it is 1.3°. In **I**, the dihedral angle between the planes defined by C7/N1/C1/C6/S1 and C7/N2/C8/C10 is

1.94 (4)° while the corresponding dihedral angle in the others vary from 13.64° in **III** to 0.61° in **V**.

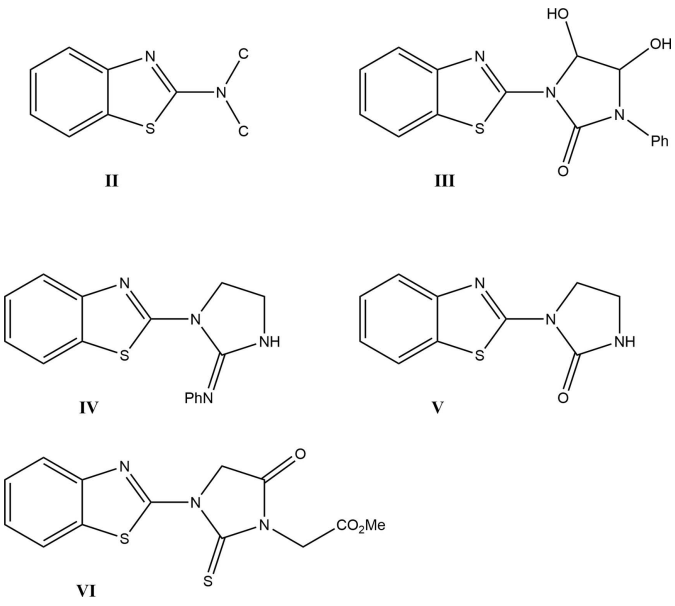

8. Synthesis and crystallization

To a mixture of 2-aminobenzothiazole (2.22 mmol), bis(2-chloroethyl)amine (1.11 mmol) and potassium carbonate (3.21 mmol) in DMF (25 mL) was added a catalytic amount of tetra-*n*-butylammonium bromide (0.37 mmol). The mixture was stirred at 353 K for 24 h. The solid material was removed by filtration and the solvent evaporated *in vacuo*. The solid product was purified by recrystallization from ethanol to give colourless crystals (yield: 70%).

9. Refinement

Crystal data, data collection and structure refinement details are summarized in Table 4. All hydrogen atoms were located in a difference-Fourier map and their coordinates and isotropic displacement parameters refined without restraints.

Table 4
Experimental details.

Crystal data	
Chemical formula	$C_{12}H_{13}N_3O_2S$
M_r	263.31
Crystal system, space group	Monoclinic, $P2_1/c$
Temperature (K)	150
a, b, c (Å)	7.2863 (2), 13.9178 (5), 11.6156 (4)
β (°)	98.866 (1)
V (Å^3)	1163.85 (7)
Z	4
Radiation type	Cu $K\alpha$
μ (mm^{-1})	2.47
Crystal size (mm)	0.28 × 0.27 × 0.11
Data collection	
Diffractometer	Bruker D8 VENTURE PHOTON 100 CMOS
Absorption correction	Multi-scan (*SADABS*; Krause *et al.*, 2015)
T_{min}, T_{max}	0.69, 0.77
No. of measured, independent and observed [$I > 2\sigma(I)$] reflections	8781, 2246, 2160
R_{int}	0.023
(sin $\theta/\lambda)_{max}$ (Å^{-1})	0.618
Refinement	
$R[F^2 > 2\sigma(F^2)]$, $wR(F^2)$, S	0.030, 0.080, 1.06
No. of reflections	2246
No. of parameters	215
H-atom treatment	All H-atom parameters refined
$\Delta\rho_{max}$, $\Delta\rho_{min}$ (e Å^{-3})	0.20, −0.36

Computer programs: *APEX3* and *SAINT* (Bruker, 2016), *SHELXT* (Sheldrick, 2015*a*), *SHELXL2018* (Sheldrick, 2015*b*), *DIAMOND* (Brandenburg & Putz, 2012) and *SHELXTL* (Sheldrick, 2008).

Funding information

The support of NSF–MRI grant No. 1228232 for the purchase of the diffractometer and Tulane University for support of the Tulane Crystallography Laboratory are gratefully acknowledged. TH is grateful to Hacettepe University Scientific Research Project Unit (grant No. 013 D04 602 004).

References

Ayhan-Kilcigil, G., Kus, C., Çoban, T., Can-Eke, B. & Iscan, M. (2004). *J. Enzyme Inhib. Med. Chem.* **19**, 129–135.
Becke, A. D. (1993). *J. Chem. Phys.* **98**, 5648–5652.
Bénéteau, V., Besson, T., Guillard, J., Léonce, S. & Pfeiffer, B. (1999). *Eur. J. Med. Chem.* **34**, 1053–1060.
Brandenburg, K. & Putz, H. (2012). *DIAMOND*, Crystal Impact GbR, Bonn, Germany.
Bruker (2016). *APEX3*, *SAINT* and *SADABS*. Bruker AXS, Inc., Madison, Wisconsin, USA.
Ćaleta, I., Grdiša, M., Mrvoš-Sermek, D., Cetina, M., Tralić-Kulenović, V., Pavelić, K. & Karminski-Zamola, G. (2004). *Farmaco*, **59**, 297–305.
Chakib, I., El Bakri, Y., Lai, C.-H., Benbacer, L., Zerzouf, A., Essassi, E. M. & Mague, J. T. (2019). *J. Mol. Struct.* **1198**, 126910–126921.
Chakib, I., Zerzouf, A., Zouihri, H., Essassi, E. M. & Ng, S. W. (2010*a*). *Acta Cryst.* E**66**, o2842.
Chakib, I., Zerzouf, A., Essassi, E. M., Reichelt, M. & Reuter, H. (2010*b*). *Acta Cryst.* E**66**, o1096.
Delmas, F., Avellaneda, A., Di Giorgio, C., Robin, M., De Clercq, E., Timon-David, P. & Galy, J. P. (2004). *Eur. J. Med. Chem.* **39**, 685–690.
Desai, N. C., Bhavsar, A. M. & Baldaniya, B. B. (2009). *Indian J. Pharm. Sci.* **71**, 90–94.
Ellouz, M., Sebbar, N. K., Boulhaoua, M., Essassi, E. M. & Mague, J. T. (2017). *IUCrData*, **2**, x170646.
Frisch, M. J., Trucks, G. W., Schlegel, H. B., Scuseria, G. E., Robb, M. A., Cheeseman, J. R., *et al.* (2009). *GAUSSIAN-09*. Gaussian Inc., Wallingford, CT, US.
Groom, C. R., Bruno, I. J., Lightfoot, M. P. & Ward, S. C. (2016). *Acta Cryst.* B**72**, 171–179.
Harfenist, M., Soroko, E. F. & McKenzie, G. M. (1978). *J. Med. Chem.* **21**, 405–409.
Hari Narayana Moorthy, N. S., Saxena, V., Karthikeyan, C. & Trivedi, P. (2012). *J. Enzyme Inhib. Med. Chem.* **27**, 201–207.
Hathwar, V. R., Sist, M., Jørgensen, M. R. V., Mamakhel, A. H., Wang, X., Hoffmann, C. M., Sugimoto, K., Overgaard, J. & Iversen, B. B. (2015). *IUCrJ*, **2**, 563–574.
Hirshfeld, H. L. (1977). *Theor. Chim. Acta*, **44**, 129–138.
Hni, B., Sebbar, N. K., Hökelek, T., El Ghayati, L., Bouzian, Y., Mague, J. T. & Essassi, E. M. (2019). *Acta Cryst.* E**75**, 593–599.
Huang, S.-T., Hsei, I.-J. & Chen, C. (2006). *Bioorg. Med. Chem.* **14**, 6106–6119.

Jayatilaka, D., Grimwood, D. J., Lee, A., Lemay, A., Russel, A. J., Taylor, C., Wolff, S. K., Cassam-Chenai, P. & Whitton, A. (2005). *TONTO - A System for Computational Chemistry. Available at: http://hirshfeldsurface.net/*

Kaur, H., Kumar, S., Singh, I., Saxena, K. K. & Kumar, A. (2010). *DIG. J. Nanomater. Bios* **5**, 67–76.

Kok, S. H. L., Gambari, R., Chui, C. H., Yuen, M. C. W., Lin, E., Wong, R. S. M., Lau, F. Y., Cheng, G. Y. M., Lam, W. S., Chan, S. H., Lam, K. H., Cheng, C. H., Lai, P. B. S., Yu, W. Y., Cheung, F., Tang, J. C. O. & Chan, A. S. C. (2008). *Bioorg. & Med. Chem.* **16**, 3626–3631.

Kozísek, J., Ulický, L., Floch, L. & Langer, V. (1995). *Acta Cryst.* C**51**, 1429–1431.

Krause, L., Herbst-Irmer, R., Sheldrick, G. M. & Stalke, D. (2015). *J. Appl. Cryst.* **48**, 3–10.

Latrofa, A., Franco, M., Lopedota, A., Rosato, A., Carone, D. & Vitali, C. (2005). *Farmaco*, **60**, 291–297.

Mackenzie, C. F., Spackman, P. R., Jayatilaka, D. & Spackman, M. A. (2017). *IUCrJ*, **4**, 575–587.

McKinnon, J. J., Jayatilaka, D. & Spackman, M. A. (2007). *Chem. Commun.* pp. 3814–3816.

Mekhzoum, M. E. M., El Bourakadi, K., Essassi, E. M., Qaiss, A. E. K. & Bouhfid, R. (2019). *J. Mol. Struct.* **1193**, 303–309.

Mekhzoum, M. E. M., Essassi, E. M., Qaiss, A. E. K. & Bouhfid, R. (2016). *RSC Adv.* **6**, 111472–111481.

Nagarajan, S. R., De Crescenzo, G. A., Getman, D. P., Lu, H. F., Sikorski, J. A., Walker, J. L., McDonald, J. J., Houseman, K. A., Kocan, G. P., Kishore, N., Mehta, P. P., Funkes-Shippy, C. L. & Blystone, L. (2003). *Bioorg. & Med. Chem.* **11**, 4769–4777.

Naithani, D. K., Shrivastava, V. K., Barthwal, J. P., Szxena, A. K., Gupta, T. A. & Shanker, K. (1989). *Indian J. Chem.* **28B**, 990–992.

Oketani, K., Nagakura, N., Harada, K. & Inoue, T. (2001). *Eur. J. Pharmacol.* **422**, 209–216.

Olyaei, A., Abbasi, A., Ghandi, M., Salimi, F. & Eriksson, L. (2006). *Acta Cryst.* E**62**, o5326–o5327.

Pitta, E., Geronikaki, A., Surmava, S., Eleftheriou, P., Mehta, V. P. & Van der Eycken, E. V. (2013). *J. Enzyme Inhib. Med. Chem.* **28**, 113–122.

Saczewski, F., Kornicka, A. & Gdaniec, M. (2005). *Pol. J. Chem.* **79**, 115–120.

Saggu, J. S., Sharma, R., Dureja, H. & Kumar, V. (2002). *J. Indian Inst. Sci.* **82**, 177–182.

Sahoo, S. K., Jena, H. S., Majji, G. & Patel, B. K. (2014). *Synthesis*, **46**, 1886–1900.

Sebbar, N. K., Ellouz, M., Elmsellem, H., Zerzouf, A., Hlimi, F. & Essassi, E. M. (2018). *J. Mar. Chim. Heterocycl.* **17**, 179–183.

Sebbar, N. K., Mekhzoum, M. E. M., Essassi, E. M., Zerzouf, A., Talbaoui, A., Bakri, Y., Saadi, M. & Ammari, L. E. (2016). *Res. Chem. Intermed.* **42**, 6845–6862.

Shastry, C. S., Joshi, S. D., Aravind, M. B. & Veerapur, V. P. (2003). *Indian. J. Het. Chem.* **13**, 57–60.

Sheldrick, G. M. (2008). *Acta Cryst.* A**64**, 112–122.

Sheldrick, G. M. (2015*a*). *Acta Cryst.* A**71**, 3–8.

Sheldrick, G. M. (2015*b*). *Acta Cryst.* C**71**, 3–8.

Singh, M. K., Tilak, R., Nath, G., Awasthi, S. K. & Agarwal, A. (2013). *Eur. J. Med. Chem.* **63**, 635–644.

Spackman, M. A. & Jayatilaka, D. (2009). *CrystEngComm*, **11**, 19–32.

Spackman, M. A., McKinnon, J. J. & Jayatilaka, D. (2008). *CrystEngComm*, **10**, 377–388.

Tewari, A. K. & Mishra, A. (2006). *Indian J. Chem.* **45B**, 489–493.

Turner, M. J., Grabowsky, S., Jayatilaka, D. & Spackman, M. A. (2014). *J. Phys. Chem. Lett.* **5**, 4249–4255.

Turner, M. J., McKinnon, J. J., Wolff, S. K., Grimwood, D. J., Spackman, P. R., Jayatilaka, D. & Spackman, M. A. (2017). *CrystalExplorer17*. The University of Western Australia.

Turner, M. J., Thomas, S. P., Shi, M. W., Jayatilaka, D. & Spackman, M. A. (2015). *Chem. Commun.* **51**, 3735–3738.

Venkatesan, P., Thamotharan, S., Ilangovan, A., Liang, H. & Sundius, T. (2016). *Spectrochim. Acta Part A*, **153**, 625–636.

Yang, B. Q., Yang, P. H. & Zhu, A. L. (2003). *Chin. Chem. Lett.* **14**, 901–903.

supporting information

Acta Cryst. (2020). E**76**, 370-376 [https://doi.org/10.1107/S2056989020001723]

Crystal structure, Hirshfeld surface analysis and interaction energy and DFT studies of 1-(1,3-benzothiazol-2-yl)-3-(2-hydroxyethyl)imidazolidin-2-one

Mohamed Srhir, Nada Kheira Sebbar, Tuncer Hökelek, Ahmed Moussaif, Joel T. Mague, Noureddine Hamou Ahabchane and El Mokhtar Essassi

Computing details

Data collection: *APEX3* (Bruker, 2016); cell refinement: *SAINT* (Bruker, 2016); data reduction: *SAINT* (Bruker, 2016); program(s) used to solve structure: *SHELXT* (Sheldrick, 2015*a*); program(s) used to refine structure: *SHELXL2018* (Sheldrick, 2015*b*); molecular graphics: *DIAMOND* (Brandenburg & Putz, 2012); software used to prepare material for publication: *SHELXTL* (Sheldrick, 2008).

1-(1,3-Benzothiazol-2-yl)-3-(2-hydroxyethyl)imidazolidin-2-one

Crystal data

$C_{12}H_{13}N_3O_2S$
$M_r = 263.31$
Monoclinic, $P2_1/c$
$a = 7.2863$ (2) Å
$b = 13.9178$ (5) Å
$c = 11.6156$ (4) Å
$\beta = 98.866$ (1)°
$V = 1163.85$ (7) Å^3
$Z = 4$
$F(000) = 552$
$D_x = 1.503$ Mg m^{-3}
Cu $K\alpha$ radiation, $\lambda = 1.54178$ Å
Cell parameters from 7989 reflections
$\theta = 6.2$–72.3°
$\mu = 2.47$ mm^{-1}
$T = 150$ K
Block, colourless
0.28 × 0.27 × 0.11 mm

Data collection

Bruker D8 VENTURE PHOTON 100 CMOS diffractometer
Radiation source: INCOATEC IμS micro-focus source
Mirror monochromator
Detector resolution: 10.4167 pixels mm^{-1}
ω scans
Absorption correction: multi-scan (*SADABS*; Krause *et al.*, 2015)
$T_{min} = 0.69$, $T_{max} = 0.77$
8781 measured reflections
2246 independent reflections
2160 reflections with $I > 2\sigma(I)$
$R_{int} = 0.023$
$\theta_{max} = 72.3°$, $\theta_{min} = 6.2°$
$h = -9\rightarrow8$
$k = -17\rightarrow15$
$l = -14\rightarrow14$

Refinement

Refinement on F^2
Least-squares matrix: full
$R[F^2 > 2\sigma(F^2)] = 0.030$
$wR(F^2) = 0.080$
$S = 1.06$
2246 reflections
215 parameters
0 restraints
Primary atom site location: dual
Secondary atom site location: difference Fourier map
Hydrogen site location: difference Fourier map
All H-atom parameters refined

$w = 1/[\sigma^2(F_o^2) + (0.0449P)^2 + 0.4296P]$
where $P = (F_o^2 + 2F_c^2)/3$
$(\Delta/\sigma)_{max} = 0.001$

$\Delta\rho_{max} = 0.20$ e Å^{-3}
$\Delta\rho_{min} = -0.36$ e Å^{-3}

Special details

Geometry. All esds (except the esd in the dihedral angle between two l.s. planes) are estimated using the full covariance matrix. The cell esds are taken into account individually in the estimation of esds in distances, angles and torsion angles; correlations between esds in cell parameters are only used when they are defined by crystal symmetry. An approximate (isotropic) treatment of cell esds is used for estimating esds involving l.s. planes.

Refinement. Refinement of F^2 against ALL reflections. The weighted R-factor wR and goodness of fit S are based on F^2, conventional R-factors R are based on F, with F set to zero for negative F^2. The threshold expression of $F^2 > 2\text{sigma}(F^2)$ is used only for calculating R-factors(gt) etc. and is not relevant to the choice of reflections for refinement. R-factors based on F^2 are statistically about twice as large as those based on F, and R- factors based on ALL data will be even larger.

Fractional atomic coordinates and isotropic or equivalent isotropic displacement parameters (Å²)

	x	*y*	*z*	U_{iso}*/U_{eq}
S1	0.84367 (4)	0.49137 (2)	0.62655 (3)	0.02128 (12)
O1	0.88222 (13)	0.29904 (7)	0.68752 (8)	0.0249 (2)
O2	0.55711 (14)	0.04397 (7)	0.66690 (8)	0.0288 (2)
H2A	0.586 (3)	0.0432 (16)	0.745 (2)	0.055 (6)*
N1	0.67379 (15)	0.47968 (7)	0.41147 (9)	0.0191 (2)
N2	0.74321 (14)	0.33066 (7)	0.49825 (9)	0.0193 (2)
N3	0.78449 (16)	0.17939 (8)	0.55357 (9)	0.0223 (2)
C1	0.69815 (16)	0.57713 (9)	0.43706 (11)	0.0188 (3)
C2	0.63908 (18)	0.65197 (10)	0.35997 (12)	0.0241 (3)
H2	0.570 (2)	0.6355 (13)	0.2837 (16)	0.035 (4)*
C3	0.67664 (19)	0.74589 (10)	0.39635 (13)	0.0267 (3)
H3	0.637 (2)	0.7985 (14)	0.3464 (16)	0.035 (5)*
C4	0.77217 (19)	0.76532 (10)	0.50716 (13)	0.0275 (3)
H4	0.797 (2)	0.8334 (13)	0.5348 (16)	0.035 (4)*
C5	0.82913 (19)	0.69236 (10)	0.58568 (12)	0.0251 (3)
H5	0.891 (2)	0.7065 (13)	0.6624 (16)	0.032 (4)*
C6	0.79036 (17)	0.59783 (9)	0.54928 (11)	0.0201 (3)
C7	0.74425 (16)	0.42847 (9)	0.50177 (10)	0.0177 (3)
C8	0.66402 (19)	0.27650 (9)	0.39448 (11)	0.0217 (3)
H8A	0.528 (2)	0.2896 (12)	0.3761 (15)	0.031 (4)*
H8B	0.725 (2)	0.2958 (12)	0.3310 (15)	0.027 (4)*
C9	0.7093 (2)	0.17217 (10)	0.43041 (11)	0.0274 (3)
H9A	0.597 (3)	0.1309 (13)	0.4205 (16)	0.037 (5)*
H9B	0.801 (2)	0.1427 (13)	0.3901 (15)	0.036 (4)*
C10	0.81190 (17)	0.27069 (9)	0.59095 (11)	0.0189 (3)
C11	0.8591 (2)	0.09704 (10)	0.62142 (11)	0.0250 (3)
H11A	0.900 (2)	0.1210 (12)	0.6983 (15)	0.028 (4)*
H11B	0.972 (2)	0.0720 (13)	0.5935 (15)	0.031 (4)*
C12	0.7190 (2)	0.01623 (9)	0.62181 (12)	0.0256 (3)
H12A	0.784 (2)	−0.0373 (12)	0.6672 (14)	0.026 (4)*
H12B	0.681 (2)	−0.0069 (11)	0.5418 (16)	0.025 (4)*

Atomic displacement parameters (Å²)

	U^{11}	U^{22}	U^{33}	U^{12}	U^{13}	U^{23}
S1	0.0263 (2)	0.01777 (18)	0.01832 (18)	0.00109 (11)	−0.00106 (13)	−0.00110 (10)
O1	0.0344 (5)	0.0211 (5)	0.0181 (4)	0.0011 (4)	0.0003 (4)	0.0002 (3)
O2	0.0353 (5)	0.0272 (5)	0.0228 (5)	−0.0006 (4)	0.0011 (4)	0.0037 (4)
N1	0.0222 (5)	0.0164 (5)	0.0185 (5)	0.0007 (4)	0.0025 (4)	0.0010 (4)
N2	0.0259 (5)	0.0152 (5)	0.0163 (5)	−0.0001 (4)	0.0012 (4)	0.0004 (4)
N3	0.0319 (6)	0.0153 (5)	0.0183 (5)	−0.0003 (4)	−0.0002 (4)	0.0023 (4)
C1	0.0191 (6)	0.0160 (6)	0.0218 (6)	0.0007 (5)	0.0048 (4)	−0.0003 (5)
C2	0.0284 (7)	0.0198 (6)	0.0237 (6)	0.0030 (5)	0.0027 (5)	0.0023 (5)
C3	0.0312 (7)	0.0181 (6)	0.0316 (7)	0.0048 (5)	0.0073 (5)	0.0036 (5)
C4	0.0300 (7)	0.0174 (6)	0.0361 (7)	0.0016 (5)	0.0081 (6)	−0.0030 (5)
C5	0.0262 (6)	0.0204 (6)	0.0281 (7)	0.0004 (5)	0.0027 (5)	−0.0051 (5)
C6	0.0198 (6)	0.0183 (6)	0.0221 (6)	0.0017 (5)	0.0030 (5)	−0.0006 (5)
C7	0.0180 (6)	0.0166 (6)	0.0188 (6)	−0.0002 (4)	0.0041 (4)	−0.0005 (4)
C8	0.0299 (7)	0.0175 (6)	0.0168 (6)	−0.0019 (5)	0.0005 (5)	−0.0003 (5)
C9	0.0439 (8)	0.0179 (6)	0.0187 (6)	−0.0025 (6)	−0.0008 (5)	0.0003 (5)
C10	0.0220 (6)	0.0172 (6)	0.0180 (6)	0.0006 (5)	0.0046 (5)	0.0021 (5)
C11	0.0333 (7)	0.0167 (6)	0.0243 (7)	0.0038 (5)	0.0022 (5)	0.0033 (5)
C12	0.0399 (8)	0.0153 (6)	0.0210 (7)	0.0011 (5)	0.0023 (6)	0.0003 (5)

Geometric parameters (Å, º)

S1—C6	1.7448 (13)	C3—C4	1.392 (2)
S1—C7	1.7517 (12)	C3—H3	0.952 (19)
O1—C10	1.2246 (16)	C4—C5	1.385 (2)
O2—C12	1.4161 (17)	C4—H4	1.008 (18)
O2—H2A	0.90 (2)	C5—C6	1.3974 (18)
N1—C7	1.3060 (16)	C5—H5	0.954 (19)
N1—C1	1.3940 (16)	C8—C9	1.5327 (18)
N2—C7	1.3619 (17)	C8—H8A	0.997 (17)
N2—C10	1.3930 (16)	C8—H8B	0.958 (17)
N2—C8	1.4628 (16)	C9—H9A	0.993 (19)
N3—C10	1.3477 (16)	C9—H9B	0.967 (18)
N3—C11	1.4485 (16)	C11—C12	1.5194 (19)
N3—C9	1.4543 (17)	C11—H11A	0.957 (18)
C1—C2	1.3975 (18)	C11—H11B	0.992 (17)
C1—C6	1.4013 (18)	C12—H12A	0.991 (17)
C2—C3	1.388 (2)	C12—H12B	0.982 (18)
C2—H2	0.977 (19)		
S1···O1	2.7721 (10)	C1···C7^{iv}	3.4070 (17)
S1···C11^{i}	3.6700 (14)	C2···C10^{iv}	3.5859 (18)
S1···C1^{ii}	3.6552 (12)	C3···C10^{iv}	3.5928 (19)
S1···H11A^{i}	3.117 (16)	C4···C10^{ii}	3.4350 (19)
O1···C9^{iii}	3.2869 (16)	C4···C8^{iv}	3.587 (2)
O1···C8^{iii}	3.2543 (16)	C6···C7^{ii}	3.5502 (17)

O2···N1^{iii}	2.8560 (14)	C1···H2A^{vi}	2.81 (2)
O2···C3^{iv}	3.4071 (17)	C4···H8A^{iv}	2.850 (16)
O2···N3	2.9500 (15)	C5···H8A^{iv}	2.718 (15)
O1···H9B^{iii}	2.640 (17)	C9···H12B	2.830 (16)
O1···H11A	2.482 (17)	C12···H9A	2.857 (18)
O1···H8B^{iii}	2.534 (16)	H2···H9A^{vii}	2.49 (3)
O2···H9A^{v}	2.804 (19)	H2···H2A^{vi}	2.53 (3)
O2···H12B^{v}	2.803 (18)	H2A···H8B^{iii}	2.59 (3)
O2···H3^{iv}	2.601 (18)	H4···C12^{viii}	2.828 (18)
O2···H2^{iii}	2.838 (18)	H4···H12A^{viii}	2.38 (2)
N1···C12^{vi}	3.4313 (17)	H4···H12B^{viii}	2.38 (2)
N2···C5^{ii}	3.4204 (17)	H5···O1^{i}	2.557 (17)
N1···H8B	2.769 (17)	H5···H11A^{i}	2.36 (2)
N1···H2A^{vi}	1.97 (2)	H8B···H11A^{vi}	2.44 (2)
N1···H8A	2.857 (17)	H9A···H12B	2.40 (2)

C6—S1—C7	88.16 (6)	N2—C7—S1	121.60 (9)
C12—O2—H2A	106.8 (13)	N2—C8—C9	102.87 (10)
C7—N1—C1	109.77 (10)	N2—C8—H8A	109.6 (10)
C7—N2—C10	125.18 (10)	C9—C8—H8A	113.3 (10)
C7—N2—C8	122.65 (10)	N2—C8—H8B	108.6 (10)
C10—N2—C8	112.16 (10)	C9—C8—H8B	111.6 (10)
C10—N3—C11	123.10 (11)	H8A—C8—H8B	110.5 (14)
C10—N3—C9	113.37 (10)	N3—C9—C8	103.60 (10)
C11—N3—C9	122.24 (11)	N3—C9—H9A	109.4 (11)
N1—C1—C2	124.89 (12)	C8—C9—H9A	112.1 (10)
N1—C1—C6	115.18 (11)	N3—C9—H9B	108.8 (10)
C2—C1—C6	119.93 (12)	C8—C9—H9B	114.0 (11)
C3—C2—C1	118.69 (13)	H9A—C9—H9B	108.7 (15)
C3—C2—H2	123.1 (10)	O1—C10—N3	128.27 (12)
C1—C2—H2	118.2 (11)	O1—C10—N2	124.38 (11)
C2—C3—C4	120.76 (13)	N3—C10—N2	107.35 (10)
C2—C3—H3	120.8 (11)	N3—C11—C12	113.03 (11)
C4—C3—H3	118.5 (11)	N3—C11—H11A	105.6 (10)
C5—C4—C3	121.51 (13)	C12—C11—H11A	111.7 (10)
C5—C4—H4	117.3 (10)	N3—C11—H11B	111.1 (10)
C3—C4—H4	121.1 (10)	C12—C11—H11B	109.4 (10)
C4—C5—C6	117.70 (13)	H11A—C11—H11B	105.7 (14)
C4—C5—H5	120.9 (11)	O2—C12—C11	113.43 (11)
C6—C5—H5	121.4 (11)	O2—C12—H12A	111.6 (9)
C5—C6—C1	121.38 (12)	C11—C12—H12A	106.8 (9)
C5—C6—S1	128.70 (10)	O2—C12—H12B	108.1 (10)
C1—C6—S1	109.92 (9)	C11—C12—H12B	109.3 (9)
N1—C7—N2	121.45 (11)	H12A—C12—H12B	107.4 (13)
N1—C7—S1	116.94 (10)		

C7—N1—C1—C2	−179.95 (12)	C8—N2—C7—S1	−178.90 (9)
C7—N1—C1—C6	0.42 (15)	C6—S1—C7—N1	−1.36 (10)

N1—C1—C2—C3	−178.49 (12)	C6—S1—C7—N2	177.54 (10)
C6—C1—C2—C3	1.12 (19)	C7—N2—C8—C9	175.82 (11)
C1—C2—C3—C4	0.4 (2)	C10—N2—C8—C9	−5.38 (14)
C2—C3—C4—C5	−1.5 (2)	C10—N3—C9—C8	−7.90 (16)
C3—C4—C5—C6	1.1 (2)	C11—N3—C9—C8	−175.30 (11)
C4—C5—C6—C1	0.40 (19)	N2—C8—C9—N3	7.49 (14)
C4—C5—C6—S1	179.83 (10)	C11—N3—C10—O1	−8.4 (2)
N1—C1—C6—C5	178.12 (11)	C9—N3—C10—O1	−175.68 (13)
C2—C1—C6—C5	−1.53 (19)	C11—N3—C10—N2	172.01 (11)
N1—C1—C6—S1	−1.40 (13)	C9—N3—C10—N2	4.74 (15)
C2—C1—C6—S1	178.95 (9)	C7—N2—C10—O1	−0.1 (2)
C7—S1—C6—C5	−178.02 (13)	C8—N2—C10—O1	−178.84 (12)
C7—S1—C6—C1	1.45 (9)	C7—N2—C10—N3	179.53 (11)
C1—N1—C7—N2	−178.10 (11)	C8—N2—C10—N3	0.77 (14)
C1—N1—C7—S1	0.80 (13)	C10—N3—C11—C12	135.47 (13)
C10—N2—C7—N1	−178.69 (11)	C9—N3—C11—C12	−58.36 (17)
C8—N2—C7—N1	−0.05 (18)	N3—C11—C12—O2	−59.05 (15)
C10—N2—C7—S1	2.46 (17)		

Symmetry codes: (i) −*x*+2, *y*+1/2, −*z*+3/2; (ii) −*x*+2, −*y*+1, −*z*+1; (iii) *x*, −*y*+1/2, *z*+1/2; (iv) −*x*+1, −*y*+1, −*z*+1; (v) −*x*+1, −*y*, −*z*+1; (vi) *x*, −*y*+1/2, *z*−1/2; (vii) −*x*+1, *y*+1/2, −*z*+1/2; (viii) *x*, *y*+1, *z*.

Hydrogen-bond geometry (Å, º)

*Cg*1 is the centroid of the benzene ring (*A*, C1–C6).

D—H···*A*	*D*—H	H···*A*	*D*···*A*	*D*—H···*A*
O2—H2*A*···N1^{iii}	0.90 (2)	1.97 (2)	2.8560 (15)	170 (2)
C5—H5···O1^{i}	0.954 (19)	2.559 (19)	3.4439 (16)	154.3 (14)
C8—H8*B*···O1^{vi}	0.958 (17)	2.532 (16)	3.2542 (16)	132.2 (13)
C8—H8*A*···*Cg*1^{iv}	0.997 (17)	2.840 (16)	3.5646 (15)	130.0 (12)

Symmetry codes: (i) −*x*+2, *y*+1/2, −*z*+3/2; (iii) *x*, −*y*+1/2, *z*+1/2; (iv) −*x*+1, −*y*+1, −*z*+1; (vi) *x*, −*y*+1/2, *z*−1/2.